metals

MDPI

Article

The Effect of Low-Temperature Annealing and Long-Term Operation of Nuclear Power Plant Components on the Corrosion Resistance of 08CH18N10T Steel

Matúš Gavalec *, Mária Dománková, Marek Kudláč, Katarína Bártová and Gabriela Stachová

Faculty of Materials Science and Technology in Trnava, Slovak University of Technology in Bratislava, 811 07 Bratislava, Slovakia; maria.domankova@stuba.sk (M.D.); marek.kudlac@stuba.sk (M.K.); katarina.bartova@stuba.sk (K.B.); gabriela.stachova@stuba.sk (G.S.)

* Correspondence: matus.gavalec@stuba.sk

Abstract

Extending the service life of nuclear power plant components beyond their originally designed operational period requires a detailed understanding of the microstructural stability of the materials used. This study focuses on low-temperature precipitation in the austenitic stainless steel 08CH18N10T, which is employed in the main circulation piping of pressurized water reactors. During long-term operation in the temperature range of 100–320 °C, secondary phases such as $M_{23}C_6$ carbides and intermetallic phase sigma (σ) can precipitate, which can lead to local chromium depletion at grain boundaries, subsequent sensitization of the steel, and susceptibility to intergranular corrosion. The research includes the analysis of samples taken from the decommissioned V1 unit of the Jaslovské Bohunice Nuclear Power Plant, which has been in operation for 28 years. The samples were subjected to thermal aging under laboratory conditions, with an emphasis on evaluating microstructural changes and their impact on corrosion resistance. Based on the experimental results, it can be concluded that the thermal stability of all tested materials is suitable for the operation of the main circulation piping, as the service temperatures to which the main circulation piping is exposed during operation remain below the activation of precipitation that would lead to sensitization and, consequently, susceptibility to intergranular corrosion. Activation of low-temperature precipitation was observed only at 450 °C, while at temperatures up to 400 °C, the structural stability of the material was confirmed, demonstrating its suitability for operation within the specified temperature range of the nuclear power plants' main circulation piping.

Keywords: 08CH18N10T; low-temperature precipitation; intergranular corrosion; sensitization

Check for updates

Academic Editor: Renato Altobelli Antunes

Received: 1 April 2026
Revised: 28 April 2026
Accepted: 1 May 2026
Published: 3 May 2026

Copyright: © 2026 by the authors. Licensee MDPI, Basel, Switzerland. This article is an open access article distributed under the terms and conditions of the Creative Commons Attribution (CC BY) license.

1. Introduction

Currently, five nuclear power plant (NPP) units are in operation in the Slovak Republic—two at the Jaslovské Bohunice plant and three at the Mochovce plant. All five NPP units utilize Russian-designed pressured water reactors (PWRs), which are the most commonly used reactor design in the countries of the former Eastern Bloc [1,2]. The intention of the owners and the European Union is to operate these reactors beyond their originally projected service life, which is already being implemented. The original design lifetime of the reactors was 25 years, and the current objective is to extend their operational period to 100 years. This goal imposes stringent requirements on the long-term structural stability of key components, such as the main circulation piping (MCP).

Austenitic stainless steels (ASSs) are widely used in highly corrosive environments, such as in the petrochemical and chemical industries, as well as in nuclear power applications, due to their excellent corrosion resistance, strength, toughness, and weldability. Most available publications focus on the corrosion resistance of ASSs at temperatures above 600 °C, and similar emphasis is found in studies of their thermal stability, which does not reflect the actual operating conditions of NPP MCP [3–9].

During operation, the MCP is exposed to temperatures in the range of 100–320 °C, with occasional local exceedances of this range, while the primary circuit typically operates at a pressure of about 12.5 MPa, and each pump provides a characteristic coolant flow of approximately 2000–2500 m^3/h. Long-term exposure under these conditions can lead to microstructural changes that cause sensitization of the steel and increase its susceptibility to intergranular corrosion (IGC). The sensitization mechanism involves the precipitation of chromium-rich carbides (e.g., $M_{23}C_6$) [10] or the intermetallic σ-phase [11], which reduces the Cr concentration in the matrix and impairs the passive layer responsible for corrosion resistance. This process is most pronounced at grain boundaries, where local chromium depletion can lead to IGC [12–23]. The addition of stabilizing elements such as Ti, Ta, or Nb is an effective method to reduce the risk of sensitization. These elements form MC-type carbides (e.g., TiC), which preferentially bind carbon instead of chromium, thereby limiting the formation of undesirable secondary phases and reducing the risk of sensitization [24–26].

In PWR systems, including Russian-designed units, IGC or failures attributable to low-temperature thermal aging of ASSs are not considered a significant issue in practice. Nevertheless, understanding the underlying microstructural mechanisms that govern these processes remains important for reliably supporting long-term operation and lifetime extension of nuclear components.

The research focuses on monitoring microstructural changes and the associated sensitization in the ASS 08CH18N10T, using samples taken from long-term in-service components of the MCP of the decommissioned V1 unit of the Jaslovské Bohunice Nuclear Power Plant (Slovakia). The V1 plant consisted of two VVER-440/230 reactor units, commissioned in 1978 and 1980 and permanently shut down in 2006 and 2008 after 28 years of operation. Samples from never-in-service MCP material, obtained from unused spare piping segments stored at the plant site, were also included for comparison. The study was further extended by a thermal aging program applied to specimens of commercially produced 08CH18N10T material (used as experimental material in this study), commonly used for MCP components. The contribution of this work lies in expanding the understanding of low-temperature sensitization of ASSs under MCP operating conditions in NPP, which is essential for the safe operation of equipment beyond its design lifetime and for the lifetime extension of nuclear units.

2. Materials and Methods

2.1. Sample Information

For the MCP, the most used material is the ASS 08CH18N10T, which is equivalent to AISI 321. It is produced in electric arc furnaces and applied in the solution-annealed condition at 1100 °C for 1 h, followed by water quenching. This Ti-stabilized material is preferred due to its high resistance to intergranular corrosion, good weldability, and microstructural stability at operating temperatures around 300 °C, including long-term thermal exposure. The chemical compositions of the never-in-service MCP material (MCP-N) and the material that had been in service for 28 years (MCP-V1) are shown in Table 1.

Table 1. Chemical composition of MCP-N and MCP-V1.

Sample	Element	C	Mn	Si	Ni	Cr	P	S	Ti	Mo	Co	Fe
MCP-N	wt. %	0.06	1.21	0.46	12.50	17.89	0.01	0.002	0.57	0.04	0.03	balance
MCP-V1	wt. %	0.05	1.05	0.59	12.59	17.79	0.01	0.003	0.54	0.06	0.03	balance

The chemical composition of the experimental 08CH18N10T steel used for the thermal aging program is shown in Table 2.

Table 2. Chemical composition of the experimental 08CH18N10T.

Sample	Element	C	Mn	Si	Ni	Cr	P	S	Ti	Fe
08CH18N10T	wt. %	0.07	1.42	0.48	10.90	19.10	0.01	0.01	0.66	balance

2.2. Heat Treatment

The experimental samples were subjected to isothermal annealing at 350, 400 and 450 °C with holding times of 1000, 2000 and 3000 h for the 08CH18N10T steel, monitored within the thermal aging program. All annealing treatments were performed in an electric laboratory furnace with a heating rate of 10 °C/min. After reaching the target temperature, the samples were held isothermally for the prescribed times and subsequently cooled inside the switched-off furnace (furnace cooling). The annealed samples were subsequently analyzed to enable a detailed study of the precipitation processes. The MCP-N and V1 materials were exposed to isothermal annealing at 350, 400 and 450 °C for 1000 h to assess their structural stability.

Table 3 presents the designation and characteristics of the individual materials used in the experimental program, together with the corresponding applied heat treatments.

Table 3. Designation and characteristics of the materials used.

Designation	Description	Heat Treatment
MCP-N	Never-in-service MCP material Initial condition	350 °C/1000 h
		400 °C/1000 h
		450 °C/1000 h
MCP-V1	MCP material after 28 years in-service Initial condition	350 °C/1000 h
		400 °C/1000 h
		450 °C/1000 h
08CH18N10T	Experimental 08CH18N10T steel used for the thermal aging program Initial condition	350 °C/1000 h
		400 °C/1000 h
		450 °C/1000 h
		350 °C/2000 h
		400 °C/2000 h
		450 °C/2000 h
		350 °C/3000 h
		400 °C/3000 h
		450 °C/3000 h

The following methods were used to analyze the samples to provide a comprehensive evaluation of microstructural changes and corrosion resistance.

2.3. Optical Microscopy (OM)

The microstructure of the samples was observed using a Zeiss Neophot 32 optical microscope (Carl Zeiss, Jena, Germany) after applying the corrosion test. Sample preparation included: wet grinding (grit sizes: 240, 600, and 1200), polishing with diamond suspension (9 µm and 3 µm), and etching according to ASTM A262, Method A (90 s in 10% oxalic acid solution, 10 V, and 1 A/cm^2) [27].

The etching pattern of the microstructure is classified into three grades according to the standard [27]:

1. Step structure—no carbides at grain boundaries.
2. Dual structure—partial precipitation.
3. Ditch structure—complete sensitization (ditches surrounding entire grains).

Microstructures with step or dual structure are classified as non-sensitized. Microstructures with ditch structure are classified as sensitized and susceptible to IGC.

2.4. Quantitative Analysis of the Fraction of Grain Boundaries with Observed Precipitation

Optical microscopy did not reveal any significant microstructural differences between the individual tested conditions. Nevertheless, the experimental matrix was extended to include a statistical evaluation of the fraction of grain boundaries exhibiting transition-type and step-type etching after the corrosion test, to obtain a more comprehensive picture of the microstructural state after the thermal aging monitoring program. A percentage ratio was determined between the length of grain boundaries affected by precipitation and those that remained unaffected

$$P = \frac{l_{GBP}}{l_{GB}} \times 100\% \quad (1)$$

P is the proportion of grain boundaries with observed precipitation, l_{GBP} is the length of grain boundaries with observed precipitation, and l_{GB} is the total length of grain boundaries.

The analyzed area on each sample was 4.5×10^6 µm^2, which represents a sufficiently large surface for reliable statistical evaluation.

2.5. Microhardness Testing

Microhardness (HV 1) was performed using a QATM QNESS 10A device (QATM GmbH, Mammelzen, Germany) following the Vickers method. Ten indents were made on each sample, after which the mean value and standard deviation were calculated.

2.6. Transmission Electron Microscopy (TEM)

TEM observations were performed using a Philips CM 300 transmission electron microscope (Philips/FEI, Eindhoven, The Netherlands) operated at an accelerating voltage of 200 kV. TEM was employed for detailed analysis of precipitates at grain boundaries, dislocation density, and particle morphology. Thin foil preparation for TEM included: mechanical thinning to 80–50 µm, punching disks (Ø 3 mm), and electrolytic thinning (Tenupol 5, 7 CH_3OH + 3 HNO_3 solution, 15 V, −35 °C). TEM analysis was further extended by selected area electron diffraction (SAED) to identify individual structural components.

Microstructures were documented in bright field (BF) and dark field (DF) modes.

2.7. Electrochemical Potentiokinetic Reactivation Test (DL-EPR)

DL-EPR measurements were performed using a GillAC potentiostat (ACM Instruments, Manchester, UK). The etching pattern classified after the ASTM A262 corrosion test only had indicative significance; therefore, experiments were extended to DL-EPR, a more precise method for quantifying the degree of sensitization (DOS) of experimental samples. The electrochemical double-loop potentiokinetic reactivation test method was used. The

principle of the method lies in monitoring current density between a Pt electrode and the sample in a corrosive environment under controlled potential variation. The DL-EPR test was performed in an electrolyte of 2 M H_2SO_4 + 0.05 M KSCN at 25 °C, using a scan rate of 100 mV/min and potential ranges of −700 mV to +500 mV for MCP and −750 mV to +500 mV for 08CH18N10T. The test consists of two steps:

1. Anodic scan—activation of the steel surface.
2. Reactivation scan—reactivation after passivation.

During the test, the peak current densities during activation (I_A) and reactivation (I_R) are recorded. The degree of sensitization is expressed as the ratio I_R/I_A and classified according to BS EN ISO 12732 [28]:

- <1%—non-sensitized sample;
- 1–5%—slightly sensitized;
- 5%—sensitized sample [29–32].

3. Results

3.1. Results of the Optical Microscopy

The microstructure of the MCP-N and MCP-V1 materials, documented in Figure 1a,b, represents the initial state after the ASTM A262 corrosion test, Method A. The microstructure exhibits a polyhedral character, with the matrix formed by austenite, and shows pronounced heterogeneity in grain size, ranging from 15 to 250 µm. In addition to the austenitic matrix, MC-type carbides were observed, and in some grains, the presence of annealing twins was also noted. No banded δ-ferrite was observed.

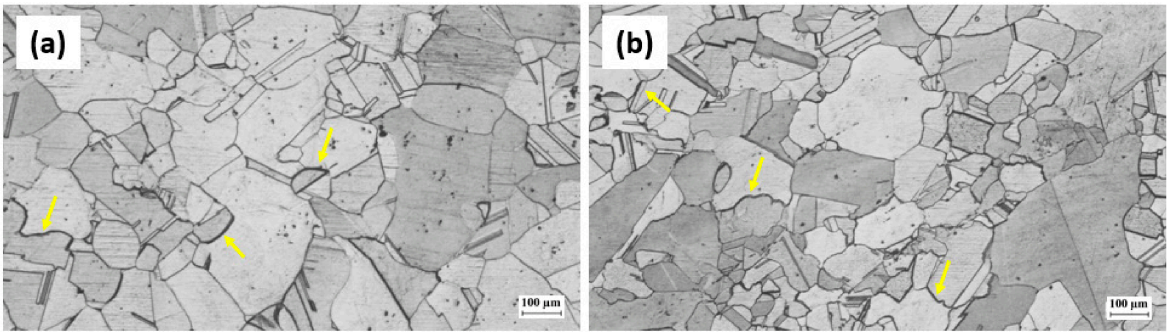


Figure 1. Microstructure of MCP samples in initial state after ASTM A262, Practice A corrosion test: (**a**) MCP-N, (**b**) MCP-V1. Yellow arrows indicate locally intensified grain-boundary etching in the form of individual pits associated with the presence of precipitates.

The microstructure of the MCP-N in the initial condition after the corrosion test (Figure 1a) exhibits a dual structure, indicating more intensive etching of certain grain boundaries (Figure 1, marked with a yellow arrow) in the form of individual pits, most likely due to the presence of precipitates. The microstructure of the MCP-V1 material in the initial condition after the corrosion test (Figure 1b) shows a very similar etching response to that of the MCP-N samples, which suggests that, despite long-term operation, no significant microstructural changes associated with sensitization or increased susceptibility to IGC were observed. Both microstructures are therefore classified as non-sensitized.

The microstructure of the experimental 08CH18N10T steel used in the thermal aging monitoring program in the initial condition is shown in Figure 2. It has a polyhedral character, with the matrix consisting of austenite and stringer-type δ-ferrite. The grain boundaries exhibit a step structure.

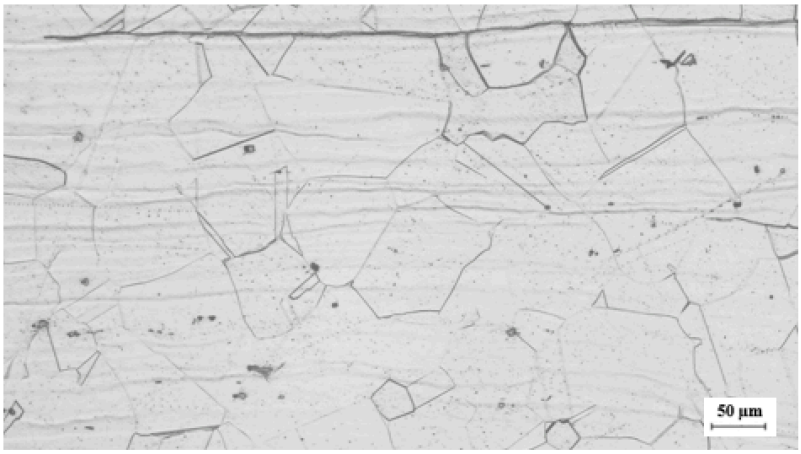


Figure 2. Microstructure of 08CH18N10T in the initial state after ASTM A262, Practice A corrosion test.

The thermal aging monitoring program applied to MCP-N material samples, after isothermal exposure at 350 °C and 400 °C for 1000 h, showed only negligible changes in the microstructure etching pattern after the corrosion test. At the highest tested exposure parameters, 450 °C for 1000 h (Figure 3a), the etching pattern after the corrosion test remained dual, but compared to the initial state of the material, a slight change in the extent of etching was observed. At the austenitic grain boundaries, individual pits can be seen, formed after etching at locations where particles precipitated (Figure 3b).

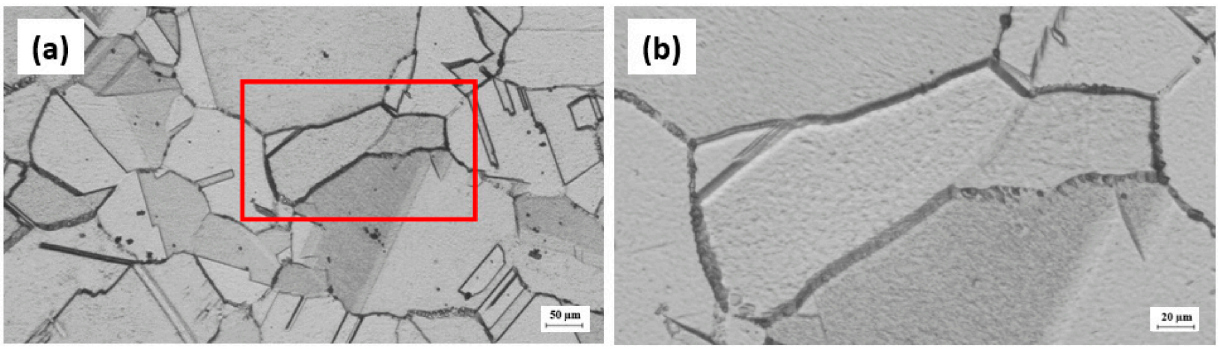


Figure 3. (**a**) Microstructure of MCP-N after isothermal annealing at 450 °C for 1000 h, (**b**) detail on the marked area.

The thermal aging program was also applied to the MCP-V1 material to verify the microstructural stability of a material that had been exposed to real MCP operating conditions for 28 years (Figure 4). Isothermal exposure of MCP-V1 samples at 350 °C (Figure 4a) and 400 °C for 1000 h did not show significant changes in the microstructure etching pattern after the corrosion test. The etching pattern of MCP-V1 samples exposed to 450 °C for 1000 h (Figure 4b), in terms of intensity and extent of grain boundary etching, is very similar to that of MCP-N material under the same conditions (450 °C/1000 h). Based on this, it can be concluded that the material used in actual operation was not exposed to temperatures of 450 °C, as thermal activation occurred in both compared materials only during exposure to 450 °C and to approximately the same extent. The microstructure also retained a dual structure; therefore, it cannot be considered sensitized or susceptible to IGC.

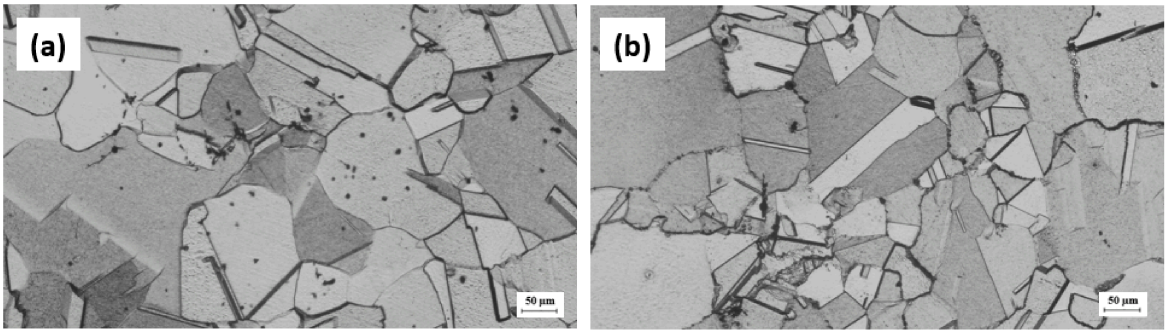


Figure 4. Microstructure of MCP-V1 samples after isothermal annealing for 1000 h, according to ASTM A262, Practice A corrosion test: (**a**) 350 °C, (**b**) 450 °C.

The microstructure of the experimental 08CH18N10T steel after isothermal annealing at 450 °C is shown in Figure 5. Figure 5a shows only step etching of the grain boundaries, while Figure 5b shows ditch etching of the grain boundaries. The most pronounced microstructural changes after applying the thermal aging monitoring program to the 08CH18N10T steel were, as expected, observed at the highest test temperature and the longest exposure time of 3000 h.

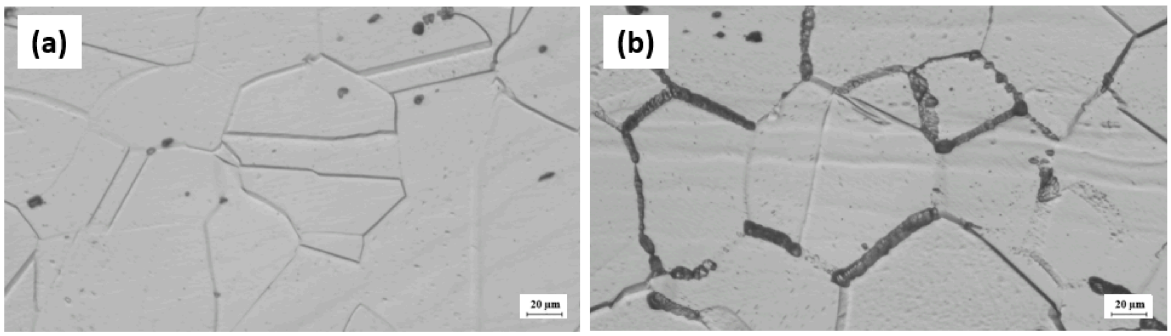


Figure 5. Microstructure of 08CH18N10T after isothermal annealing at 450 °C, according to ASTM A262, Practice A corrosion test: (**a**) 1000 h, (**b**) 3000 h.

Despite the most pronounced microstructural changes, the experimental material 08CH18N10T was evaluated as highly phase-stable even after isothermal annealing with a holding time of 3000 h at all tested temperatures. Nevertheless, more intensive etching was observed at the austenite/δ-ferrite interface and at some grain boundaries at 450 °C. However, the etching structure did not change and remained dual. Only localized ditch etching appeared in certain regions, but this does not meet the criteria for a full ditch structure as defined by the applied classification standard. Such an etched microstructure cannot be considered sensitized or susceptible to IGC.

3.2. Results of the Quantitative Analysis of the Fraction of Grain Boundaries with Observed Precipitation

The corrosion test did not indicate sensitization in any of the samples examined; therefore, a more detailed differentiation of the conditions was carried out using statistical analysis. The results of the quantitative evaluation of the fraction of grain boundaries containing precipitates were divided into two graphs. Figure 6 presents the graphical assessment of the results for the MCP-N and MCP-V1 samples.

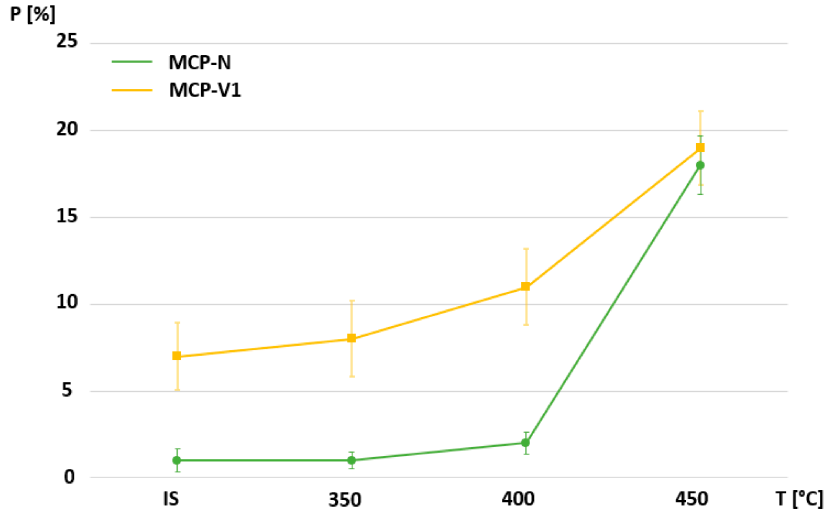


Figure 6. Quantitative analysis of grain boundary precipitation in MCP-N and MCP-V1 samples.

Given the long-term operation of the MCP-V1 sample in its initial condition, a slight increase in the percentage of affected grain boundaries may be expected. A more pronounced percentage of grain boundaries with precipitation for both tested materials was observed at 450 °C/1000 h. The proportion of grain boundaries with precipitates is very similar, which indicates excellent phase stability of the steel.

Figure 7 shows the graphical evaluation of results from the statistical analysis of the proportion of grain boundaries where precipitation was observed for samples of the experimental material 08CH18N10T.

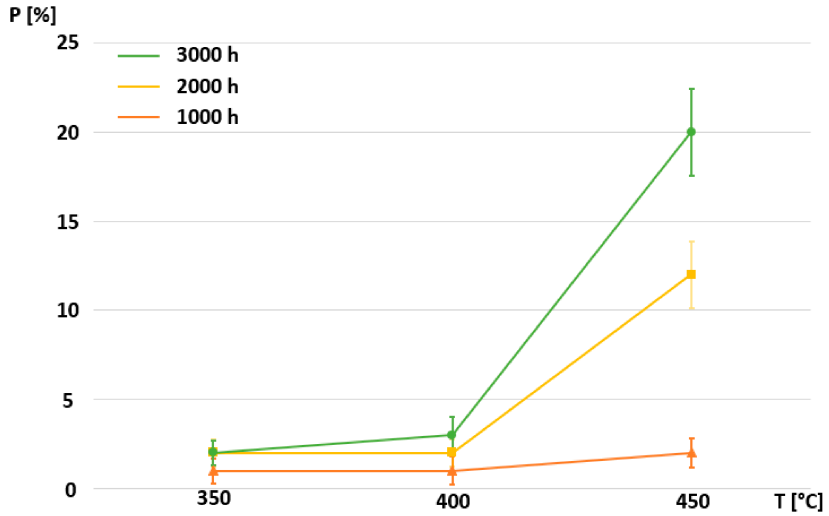


Figure 7. Quantitative analysis of grain boundary precipitation in 08CH18N10T samples.

As with the MCP samples, the most significant activation of precipitation was observed at the highest tested temperature, 450 °C. The most pronounced precipitation activation occurred after more than 1000 h of exposure at the maximum tested temperature.

3.3. Results of the Microhardness Testing

Microhardness measurements were performed to determine potential changes in mechanical properties caused by long-term service or applied thermal aging.

Figure 8 shows the graphically represented microhardness values for individual samples. These values represent the average microhardness and standard deviation from ten measurements for samples MCP-N and MCP-V1.

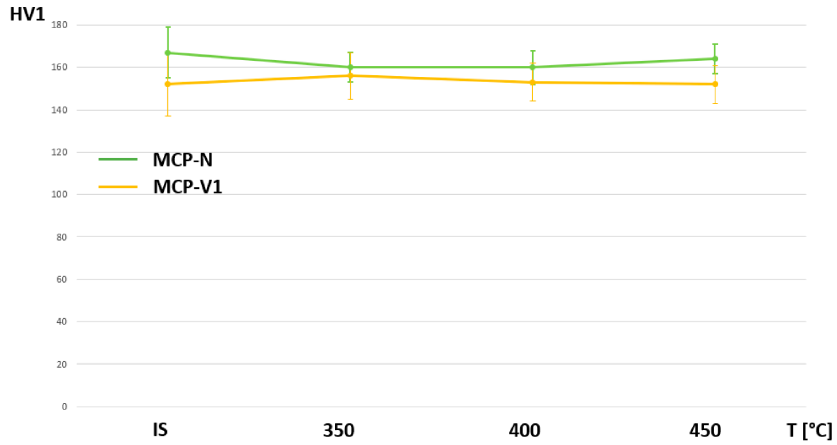


Figure 8. Microhardness test results for MCP-N and MCP-V1 samples.

Based on the results presented, there are no significant differences in values between the individual samples.

Microhardness testing was also carried out for samples subjected to the thermal aging program of 08CH18N10T material. Graphically represented results of average microhardness and standard deviation from ten measurements are shown in Figure 9.

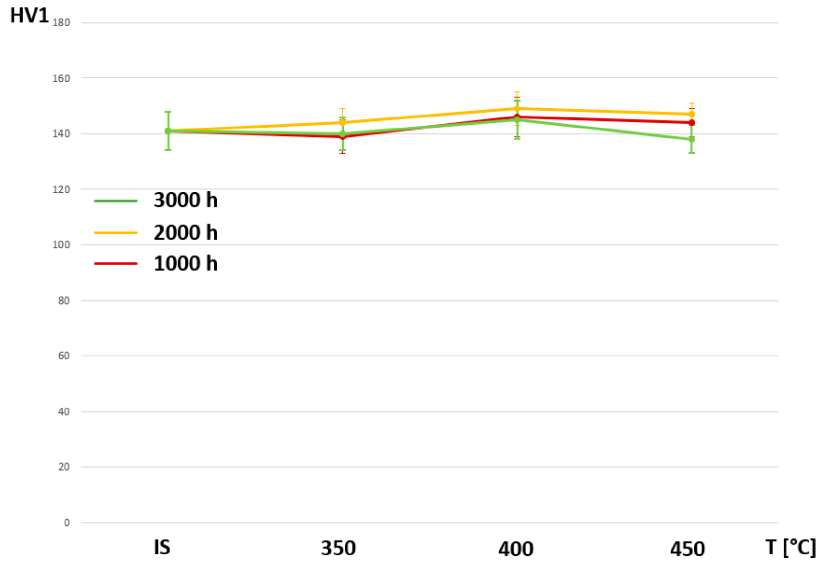


Figure 9. Microhardness test results for 08CH18N10T samples.

The tested temperatures and exposure times did not demonstrate any significant influence on the microhardness of 08CH18N10T steel. The measured deviations, as in the case of MCP materials, were within the tolerance of measurement error.

3.4. Transmission Electron Microscopy

Based on the observations and analysis of the OM images, a gradual increase in the proportion of thickened grain boundaries was confirmed with increasing aging parameters, suggesting the presence of undesirable secondary phases. The experimental program was therefore extended to include TEM, as this technique is well-suited for identifying secondary phases expected to form during low-temperature precipitation in the investigated steels.

An overview TEM micrograph of the experimental 08CH18N10T material is shown in Figure 10. No particles attributable to undesirable precipitation were detected at the grain boundaries. An increased dislocation density is observed both along the grain boundaries and within the austenitic matrix.

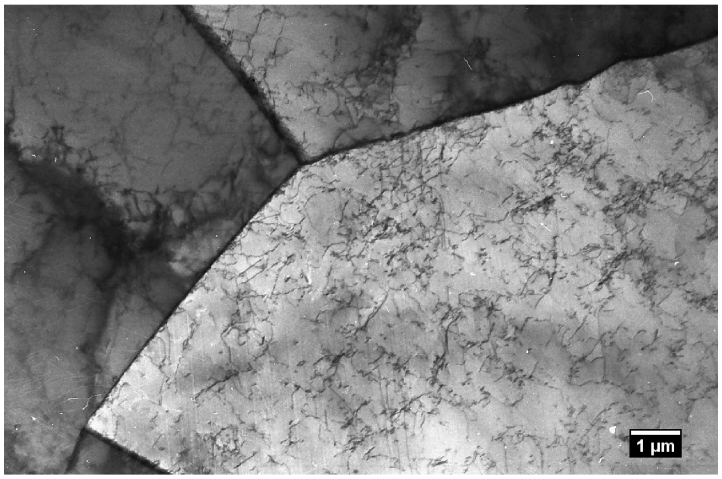


Figure 10. 08CH18N10T sample 350/1000—overview micrograph of the microstructure.

The following images document the individual phases identified in the selected samples. In addition to the austenitic matrix, the σ phase was identified in the initial microstructure of the MCP-N material. A coarse isolated particle (Figure 11a,b) located at the grain boundary was identified as the σ phase using the SAED (Figure 11c).

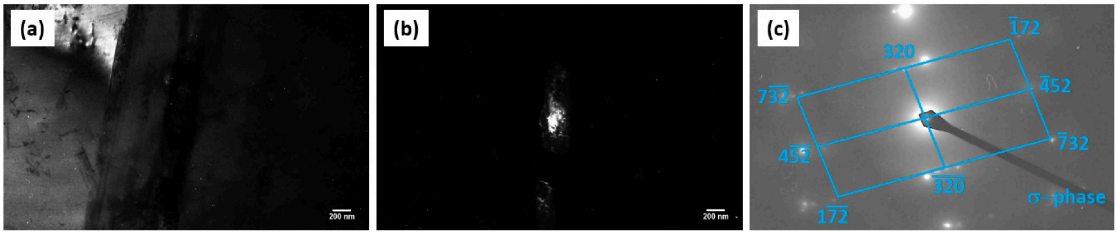


Figure 11. MCP-N, initial condition: (**a**) detail of a coarse particle at the grain boundary (BF), (**b**) detail of a coarse particle at the grain boundary (DF), (**c**) evaluated spot diffraction pattern of the σ phase.

In the MCP N samples exposed to the thermal aging program at the lowest tested temperature of 350 °C for a holding time of 1000 h, precipitation of individual secondary particles was also observed at grain boundaries (Figure 12a,b) as well as at subgrain boundaries. Using electron diffraction (Figure 12c), the presence of $M_{23}C_6$ carbide was confirmed.

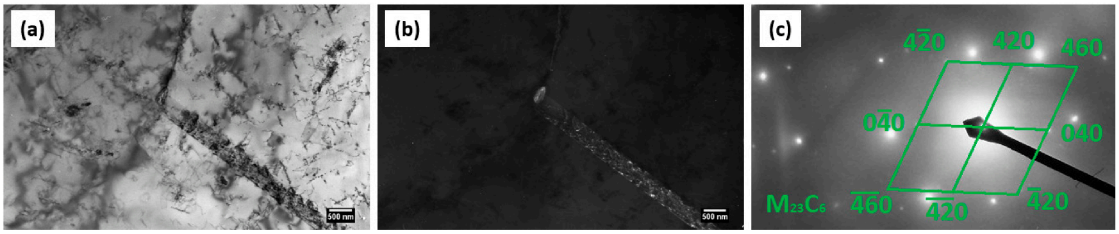


Figure 12. MCP-N 350/1000: (**a**) detail of particles at the grain boundary (BF), (**b**) detail of particles at the grain boundary (DF), (**c**) evaluated spot diffraction pattern of the $M_{23}C_6$ carbide.

Precipitation of the $M_{23}C_6$ carbide was observed at subgrain boundaries (Figure 13a,b) in the initial condition of the MCP-V1 samples. Electron diffraction confirmed the presence of the $M_{23}C_6$ carbide (Figure 13c).

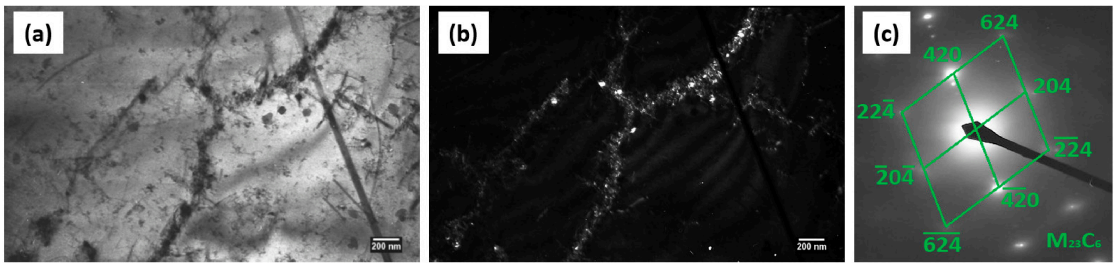


Figure 13. MCP-V1, initial condition: (**a**) detail of particles at subgrain boundaries (BF), (**b**) detail of particles at subgrain boundaries (DF), (**c**) evaluated spot diffraction pattern of the $M_{23}C_6$ carbide.

In the 08CH18N10T samples examined by TEM within the thermal aging program, no precipitation of secondary phases was observed in the initial microstructural condition, in contrast to the initial states of the MCP-N and MCP-V1 samples. TEM analysis of the initial condition of the 08CH18N10T material confirmed the presence of an austenitic matrix, TiC carbide, and δ-ferrite. Secondary phases were observed for the first time by TEM in the sample exposed to 450 °C for 2000 h. In all samples annealed at 450 °C for 2000–3000 h within the thermal aging program, the σ phase and $M_{23}C_6$ carbide were identified.

The evolution of the microstructure in the experimental 08CH18N10T steel throughout the thermal aging program is illustrated in Figure 14, with particular attention given to changes occurring at the grain boundaries.

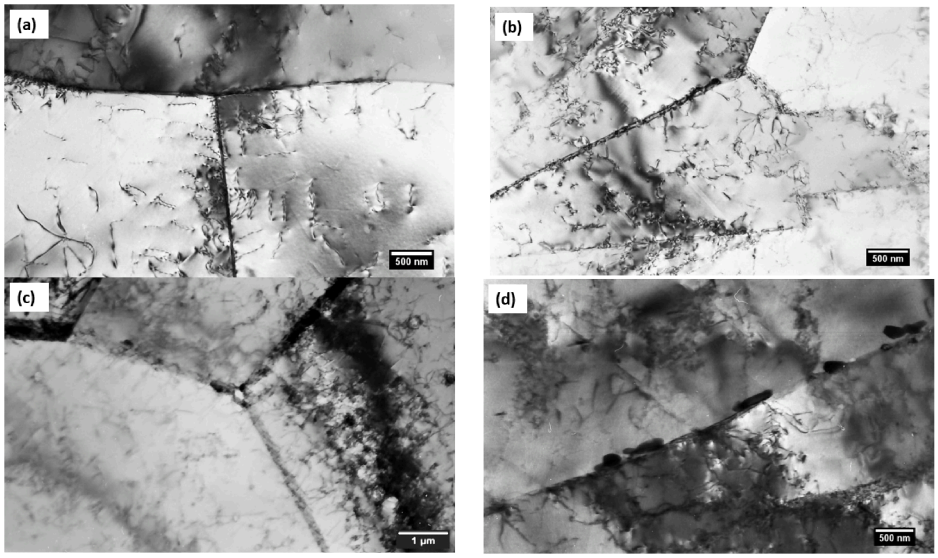


Figure 14. The evolution of the microstructure in the experimental 08CH18N10T steel observed by TEM: (**a**) 350 °C/2000 h detail of the triple point—grain boundaries are clean without the presence of precipitates; (**b**) 400 °C/2000 h detail of several boundaries of austenitic grains without precipitates; (**c**) 450 °C/2000 h detail of the small particle in triple point; (**d**) 450 °C/3000 h—small particles of irregular shape at the grain boundary.

3.5. Results of the DL-EPR Test

Based on the DL-EPR test results, the degree of sensitization (DOS) of selected samples was quantified. In the first stage, the DL-EPR test was performed on MCP-N and MCP-V1 samples. DL-EPR specifications for MCP-N, MCP-V1: Electrolyte: 2 M H_2SO_4 + 0.05 M KSCN [32], scan rate: 100 mV/min, measurement range: −700 mV to 300 mV and back, measured area: ±30 mm^2; prior to the test, a 30 min OCP (Open Circuit Potential) measurement was conducted. Figure 15 shows the measured DL-EPR curves for the

MCP-N and MCP-V1 samples. Table 4 presents the DL-EPR test results for the MCP-N and MCP-V1 samples.

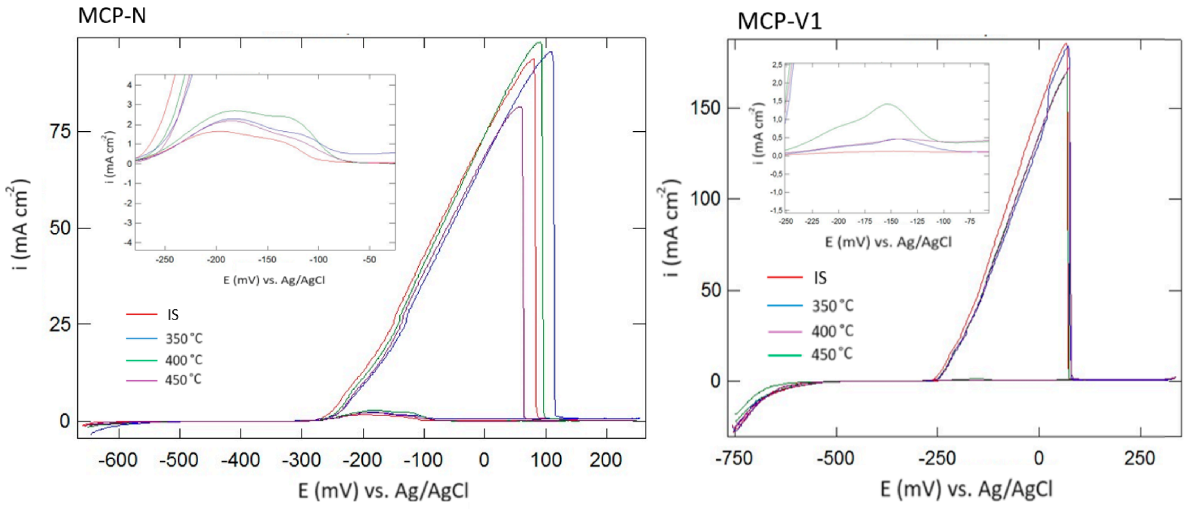


Figure 15. DL-EPR measurement results for MCP-N and MCP-V1 samples; i—current density [mA·cm^{-2}], E vs. Ag/AgCl—measured potential vs. Ag/AgCl reference electrode [mV].

Table 4. DL-EPR test results for MCP-N and MCP-V1 samples.

Sample	I_A [mA cm^{-2}]	I_R [mA cm^{-2}]	DOS [%]	Classification
MCP-N IS	152.59	0.1880	0.123	Non-sensitized
MCP-N 350 °C	152.72	0.1741	0.114	Non-sensitized
MCP-N 400 °C	159.54	0.5744	0.360	Non-sensitized
MCP-N 450 °C	177.00	0.6669	0.377	Non-sensitized
MCP-V1 IS	185.23	0.1258	0.068	Non-sensitized
MCP-V1 350 °C	184.06	0.4634	0.252	Non-sensitized
MCP-V1 400 °C	172.14	0.4644	0.270	Non-sensitized
MCP-V1 450 °C	169.34	1.4144	0.835	Non-sensitized

All tested MCP-N samples are classified as non-sensitized according to the applied scale. The initial microstructure sample is also evaluated as non-sensitized, and the difference compared to samples subjected to isothermal annealing is only minor.

The tested MCP-V1 samples already exhibited a lower percentage of DOS in the initial condition. Although isothermal annealing increased the DOS, the increase was not sufficient to change the sensitization classification. All tested MCP-V1 samples were therefore classified as non-sensitized.

In the second stage of testing, the DL-EPR test was also performed on all samples of 08CH18N10T material within the thermal aging monitoring program. To improve curve resolution, the measurement range was adjusted to −750 mV to 500 mV, while other parameters remained unchanged. The measured DL-EPR curves for 08CH18N10T material are shown in Figure 16.

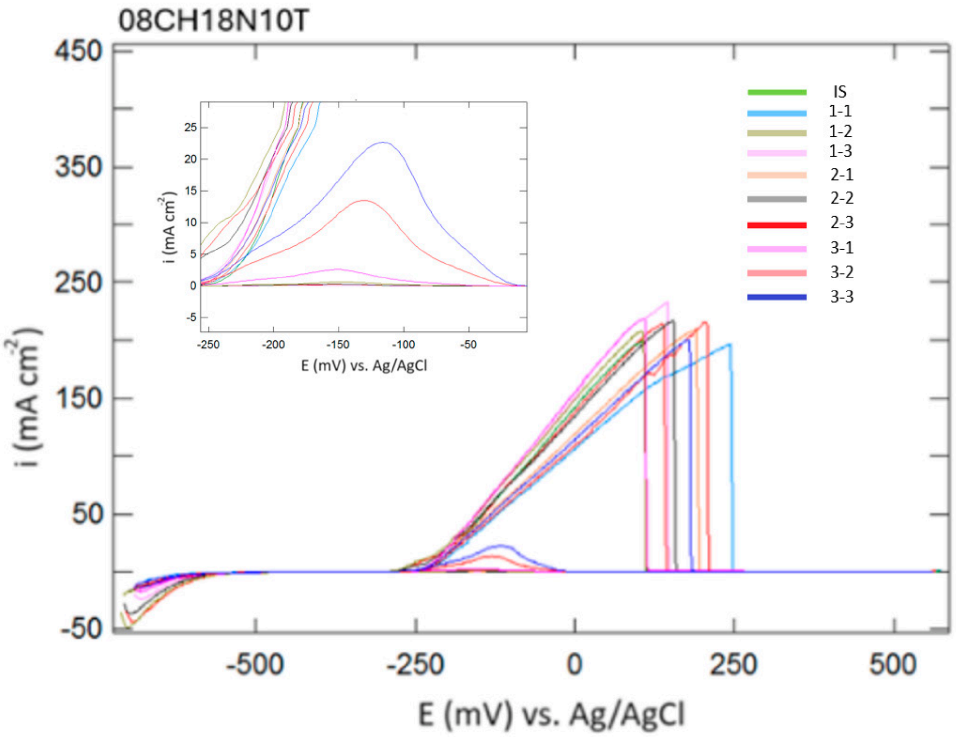


Figure 16. DL-EPR measurement for 08CH18N10T samples.

Test results together with the calculated DOS and classification of sensitization are presented in Table 5.

Table 5. DL-EPR test results for 08CH18N10T samples.

08CH18N10T	I_A [mA cm^{-2}]	I_R [mA cm^{-2}]	DOS [%]	Classification
Initial stage	213.942	0.219	0.102	Non-sensitized
350 °C/1000 h (1-1)	196.343	0.120	0.061	Non-sensitized
350 °C/2000 h (1-2)	198.481	0.126	0.063	Non-sensitized
350 °C/3000 h (1-3)	224.992	0.089	0.040	Non-sensitized
400 °C/1000 h (2-1)	208.99	0.241	0.115	Non-sensitized
400 °C/2000 h (2-2)	216.471	0.274	0.127	Non-sensitized
400 °C/3000 h (2-3)	207.13	0.633	0.306	Non-sensitized
450 °C/1000 h (3-1)	217.854	2.582	1.185	Slightly sensitized
450 °C/2000 h (3-2)	215.54	13.474	6.251	Sensitized
450 °C/3000 h (3-3)	216.471	22.645	10.461	Sensitized

Samples of 08CH18N10T material tested at the highest temperature of 450 °C exhibited some degree of sensitization compared to samples tested at other temperatures, regardless of exposure time. These results are in good agreement with those obtained by optical microscopy, where an increase in sensitization and the proportion of grain boundaries affected by precipitation was also observed at the highest tested temperature of 450 °C.

To provide a clearer view of the microstructural condition of the 08CH18N10T samples after the DL-EPR test, Figure 17a shows the microstructure in the initial stage, while Figure 17b presents the microstructure after the application of the thermal aging monitoring program (450 °C/3000 h). The grain boundaries in the initial microstructure do not exhibit

any features indicating the precipitation of secondary particles. In contrast, the micrograph of the sample exposed to the highest parameters of the thermal aging program shows pronounced grain-boundary attack, indicating ongoing precipitation.

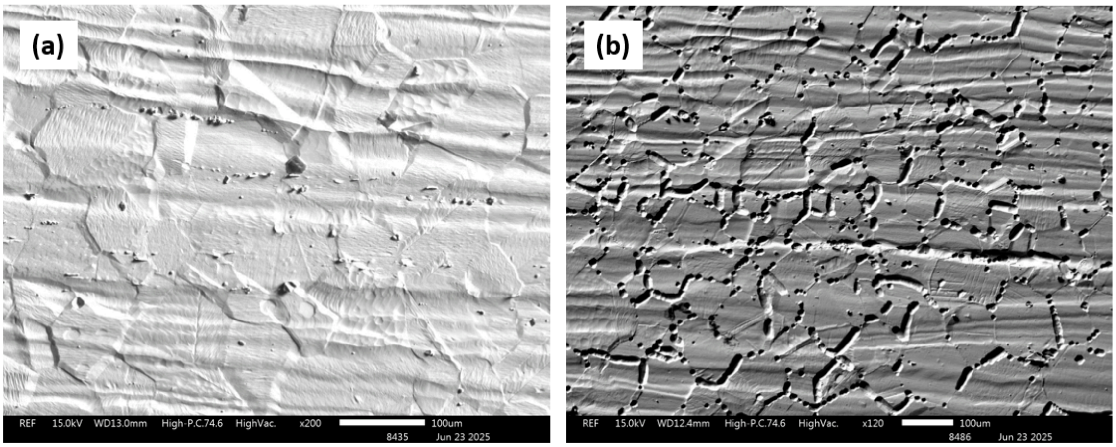


Figure 17. Microstructure of the 08CH18N10T sample after the DL-EPR test: (**a**) initial microstructural condition, (**b**) after isothermal annealing at 450 °C for 3000 h.

4. Discussion

ASSs generally exhibit the highest corrosion resistance among stainless steel grades. However, practical experience shows that susceptibility to sensitization and the resulting IGC, initiated by the precipitation of secondary phases, can compromise this resistance. The low-temperature sensitization range [33,34] of ASSs is relatively poorly investigated, as most studies focus on temperatures above 600 °C [35–38]. Nevertheless, considering the current trend of extending the service life of NPP beyond their original design lifetime, it is necessary to verify whether their operation—and any potential lifetime extension—continues to meet the required safety standards.

Optical microscopy findings. Initial information on the microstructural character of the experimental steels was obtained using OM. No significant difference was observed between the microstructures when comparing the extent of precipitation in the initial condition, the material that had been in service for 28 years (MCP-V1) and the never-in-service material (MCP-N). Microstructures of both materials were evaluated as non-sensitized. The microstructure of MCP-V1 and MCP-N samples did not differ substantially, which suggests excellent phase stability of the selected material, even after nearly 30 years of operation. That was also confirmed by the statistical evaluation of grain boundaries with precipitates. The observed difference was approximately 6%. The highest proportion of grain boundaries with precipitates was recorded at the highest temperature of 450 °C/1000 h, which was very similar for both tested materials. This suggests that the experimental steel responds to elevated temperatures in the same way, regardless of whether it was new or previously in-service. Based on the observations of MCP-V1 samples, it can be concluded that the material was not exposed to temperatures of 400 °C or 450 °C during service. Although such temperatures are well above normal operating conditions and are not expected to occur in service, they were included in the thermal aging program to accelerate phase transformations and to establish a reference for comparison with the in-service sample. Phase stability of MCP-N and MCP-V1 samples began to deteriorate at 400 °C and was significantly affected at 450 °C.

Within the thermal aging monitoring program, the microstructure of MCP-N and MCP-V1 samples was compared with samples of the experimental material 08CH18N10T, which contained δ-ferrite.

Despite the presence of δ-ferrite in 08CH18N10T samples and the preferential formation of secondary phases on δ-ferrite, no significant negative effect on material sensitization was observed. Extensive application of the thermal aging monitoring program to the experimental material 08CH18N10T confirmed phase stability degradation at 450 °C.

The results of the statistical analysis of grain boundaries affected by precipitation in MCP-V1 and MCP-N samples at 450 °C/1000 h were comparable to those of 08CH18N10T samples under the same temperature regime and a holding time of 3000 h. Based on the corrosion test, it can be concluded that the tested materials are suitable for MCP application, as no significant microstructural changes occur at operating temperatures.

Microhardness Testing. Microhardness measurements also confirmed that no significant microstructural changes occurred that would affect mechanical properties.

TEM and Electron Diffraction Findings. The presence of secondary phases was confirmed even in the initial condition of the never-in-service MCP-N material. Their occurrence in both MCP samples (in-service and never-in-service) is attributed to the manufacturing and heat-treatment history of the cast components, rather than to exposure to elevated temperatures during service. It should be emphasized that TEM can detect nanoscale σ and $M_{23}C_6$ precipitates that remain below the resolution limit of OM. These phases form very fine, discontinuous particles that do not produce visible etching or contrast changes in OM. Therefore, TEM reveals the early stages of precipitation, which removes the apparent discrepancy between the two techniques. Primary precipitation sites were grain boundaries, subgrain boundaries, and δ-ferrite, as reported in [39–42]. Secondary phases identified in the experimental steel included $M_{23}C_6$ carbide and the σ phase.

DL-EPR Test Findings. DL-EPR tests performed on the MCP-V1 and MCP-N samples confirmed a degree of sensitization that is not considered a risk for the onset of IGC. In the 08CH18N10T material, some sensitization was detected only at the highest tested temperature of 450 °C. At longer exposure times at the maximum annealing temperature, the microstructure of the 08CH18N10T samples was classified as sensitized. The rapid increase in sensitization at 450 °C/2000 h and 3000 h correlates with the increase observed in the statistical analysis of the fraction of grain boundaries affected by precipitates. A suitable extension of the DL-EPR approach in future research could involve additional electrochemical tests, such as standard or cyclic potentiodynamic polarization, which would provide complementary insight into general or pitting corrosion.

Overall findings. The results obtained from the different experimental methods show very good mutual agreement. The materials maintained excellent structural stability at temperatures representative of the actual operating conditions of the MCP in NPP, as precipitation was observed only sporadically. This conclusion is further supported by the examination of material that had been exposed to approximately three decades of reactor service, confirming the long-term stability of the microstructure.

The findings demonstrate that, despite the relatively low operating temperatures in NPP MCP, precipitation can still be initiated, which highlights the importance of thoroughly evaluating these temperatures in the context of the application of ASSs. Understanding the potential for low-temperature precipitation is therefore essential for ensuring the long-term safety and reliability of components in extended-lifetime NPP operation.

5. Conclusions

The primary objective of this research was to study the effect of long-term operation on the corrosion resistance of 08CH18N10T steel, with a focus on monitoring thermal aging of ASSs. This research is focused on evaluating the microstructural stability and sensitization behavior of the investigated materials. The assessment of mechanical properties of the tested materials represents a suitable direction for future research.

Initially, samples of in-service MCP (V1) and never-in-service (N) conditions were analyzed, both in their initial stage and after heat treatment at 350, 400, and 450 °C with a holding time of 1000 h. MCP samples were compared with experimental material 08CH18N10T, which is used for NPP MCP. Based on the results obtained, the following conclusions can be drawn:

1. The corrosion test and the resulting microstructural morphology were not characterized as a ditch structure in any case. This means that even after exposure to the highest temperature, the samples were not classified as sensitized by OM.
2. Microstructural analysis based on OM confirmed a gradual increase in the proportion of secondary phases with increasing heat treatment parameters.
3. Microstructural analysis based on TEM confirmed the presence of secondary phases, specifically $M_{23}C_6$ carbide and σ phase. The presence of secondary precipitates was also confirmed in the initial condition of the never-in-service MCP-N material; however, their presence did not cause sensitization of the steel.
4. Based on these criteria and the obtained results, it can be concluded that the thermal stability of all tested materials is suitable for the operation of MCP components, as the service temperatures to which MCP is exposed during operation are below the activation threshold for precipitation that would lead to sensitization and susceptibility to IGC. Furthermore, long-term service, as monitored in the analysis of MCP-V1 material in its initial condition, did not confirm sensitization, even when parameters were exceeded to 450 °C. The results indicate that the investigated steels maintain stable microstructures at temperatures representative of real MCP operating conditions, supporting their suitability for extended service life. Although low-temperature precipitation may occur over long exposure times, its extent did not lead to sensitization or reduced corrosion resistance. These findings suggest that continued operation and potential life extension of MCP components remain safe with respect to microstructural stability. These findings were also supported by other experimental methods, such as microhardness testing, statistical analysis of grain boundaries with precipitates, and DL-EPR testing, whose results were in good agreement.

Author Contributions: Conceptualization: M.G., M.D. and M.K. Methodology: M.G., M.D., M.K., K.B. and G.S. Validation: M.G., M.K. and K.B. Formal analysis: M.G., M.D., M.K., K.B. and G.S. Writing—original draft: M.G., M.K. and M.D. Writing—review and editing: M.G., K.B. and G.S. Funding acquisition: M.D. Supervision: M.D. and K.B. Project administration: M.D. and K.B. All authors have read and agreed to the published version of the manuscript.

Funding: The research was conducted within the framework of the International Horizon-Euratom project "Lifetime Extension and Its Impact on Safety and Performance of Structural Materials—Long-Term Operation without Safety Compromises," DELISA-LTO (No. 101061201). This work was supported by the Slovak Research and Development Agency under the Contract no. APVV-22-0146.

Data Availability Statement: The original contributions presented in this study are included in the article. Further inquiries can be directed to the corresponding author.

Conflicts of Interest: The authors declare no conflicts of interest.

References

1. JAVYS. Jadrové Zariadenia—História. Available online: https://www.javys.sk/sk/jadrove-zariadenia/jadrova-elektraren-v1/historia (accessed on 1 March 2026).
2. Slugen, V.; Veterníková, J.S. Critical analysis of the primary circuit components important to LTO's safe operation of NPP VVER-440 and VVER-1000. *AIP Conf. Proc.* **2024**, *3251*, 080001.

3. Jirková, H.; Janda, T.; Růžička, J.; Mach, J.; Volkmannová, J. Effect of holding time at stabilization annealing on properties of 08CH18N10T austenitic stainless steel. In *Proceedings of the 29th International Conference on Metallurgy and Materials*; Tanger Ltd.: Brno, Czech Republic, 2020; pp. 428–433, ISBN 978-80-87294-97-0.
4. Ehrnstén, U.; Andersen, L.P.; Que, Z. A review of stress corrosion cracking of austenitic stainless steels in PWR primary water. *J. Nucl. Mater.* **2024**, *588*, 154815. [CrossRef]
5. Slugen, V.; Simeg Veternikova, J.; Domankova, M.; Gavalec, M.; Petzova, J.; Slnek, D.; Dzubinsky, M.; Shugaylo, O.; Szenthe, I.; Gillemot, F.; et al. VVER long-term operation—A review based on the material studies results from past and ongoing EU-supported research projects. *Nucl. Eng. Des.* **2025**, *435*, 113949. [CrossRef]
6. Jin, L.; Zhang, S.-L.; Wang, X.-X.; Yin, Q.-W.Y.; Zhu, M.-L.; Xuan, F.-Z. Effect of aging on the low cycle fatigue performance of a low alloy steel. *Procedia Struct. Integr.* **2024**, *52*, 12–19. [CrossRef]
7. Fekete, B.; Trampus, P.; Jandova, D.; Kasl, J.; Jóni, B.; Misják, F.; Radnóczi, G. Low cycle thermomechanical fatigue of VVER-440 reactor pressure vessel steels: Investigation of fatigue kinetics and development of a life assessment model. *Procedia Struct. Integr.* **2016**, *2*, 2164–2172. [CrossRef]
8. Materna, A.; Hausild, P.; Ondráček, J.; Adámek, J.; Petelová, P. Effects of cold-working and annealing at 700 °C on hardness of 08Ch18N10T steel. *Procedia Struct. Integr.* **2019**, *23*, 425–430. [CrossRef]
9. Grozinger, N.; Veile, G.; Herzig, M.; Weihe, S. Fatigue tests of austenitic stainless steel AISI 321 and the weld metal ER308L in air and high-temperature water environment. *Procedia Struct. Integr.* **2025**, *75*, 642–649. [CrossRef]
10. Hatakeyama, T.; Sawada, K. Precipitation behavior of the $M_{23}C_6$ phase on the coherent twin boundary of 25Cr-20Ni-Nb-N steel. *Mater. Lett.* **2024**, *363*, 136277. [CrossRef]
11. Lescur, A.; Stergar, E.; Lim, J.; Hertele, S.; Petrov, R.H. Microstructural investigation and identification of intermetallic σ phase in solution annealed 316L type austenitic stainless steel. *Mater. Charact.* **2021**, *182*, 111524. [CrossRef]
12. Eskandari, M.; Yeganeh, M.; Motamedi, M. Investigation of the corrosion behavior of bulk nanocrystalline 316L austenitic stainless steel in NaCl solution. *Micro Nano Lett.* **2012**, *7*, 380–383. [CrossRef]
13. Margolin, B.; Pirogova, N.; Sorokin, A.; Morozov, A. Correlation between grain boundary strength determined by impact test of miniature specimens and stress corrosion cracking resistance of irradiated austenitic steels used for internals of WWER type and PWR type nuclear reactors. *Eng. Fail. Anal.* **2021**, *127*, 105544. [CrossRef]
14. Kudlac, M.; Domankova, M.; Bartova, K.; Gavalec, M.; Slnek, D. Influence of final turning on SCC susceptibility and corrosion properties of austenitic stainless steel 08Ch18N10T. *J. Phys. Conf. Ser.* **2024**, *2931*, 012014. [CrossRef]
15. Bai, S.; Zhang, S.; Ma, J.; Li, J.; Mou, L. Understanding the effect of decreasing C content and increasing solid solution time on intergranular corrosion resistance of 304 austenitic stainless steel. *J. Mater. Res. Technol.* **2024**, *30*, 4750–4761. [CrossRef]
16. Fujii, T.; Suzuki, M.; Shimamura, Y. Susceptibility to intergranular corrosion in sensitized austenitic stainless steel characterized via crystallographic characteristics of grain boundaries. *Corros. Sci.* **2022**, *195*, 109946. [CrossRef]
17. Fujii, T.; Kawarabayashi, K.; Shimamura, Y. Intergranular corrosion in sensitized austenitic stainless steel subjected to tensile loading and unloading in the elastic plastic region. *Corros. Sci.* **2024**, *230*, 111896. [CrossRef]
18. Zeng, Q.; Chen, Y.; Yang, Z.; Zhang, L.; Wang, Z.; Wang, L.; Li, J.; Wang, J. Effect of grain size and grain boundary type on intergranular stress corrosion cracking of austenitic stainless steel: A phase field study. *Corros. Sci.* **2024**, *241*, 112557. [CrossRef]
19. Rahimi, S.; Marrow, T.J. A new method for predicting susceptibility of austenitic stainless steels to intergranular stress corrosion cracking. *Mater. Des.* **2020**, *187*, 108368. [CrossRef]
20. Jin, J.-C.; Cho, S.; Kim, K.; Sim, H.; Park, G.B.; Lee, Y.-K. Microstructures and intergranular corrosion resistance of hot rolled austenitic stainless steel-clad plates. *J. Mater. Res. Technol.* **2023**, *26*, 1–13. [CrossRef]
21. Mou, L.; Bian, L.; Zhang, S.; Liu, B.; Wu, P.; Zhang, J.; Yu, Y.; Zhang, Y.; Wang, X. New insights into the intergranular corrosion resistance mechanism of type 304 austenitic stainless steel by adjusting carbon content. *J. Mater. Res. Technol.* **2023**, *26*, 666–680. [CrossRef]
22. Fujii, T.; Sawada, T.; Tohgo, K.; Shimamura, Y. Mechanical criterion for nucleation of intergranular stress corrosion cracking in austenitic stainless steel. *Forces Mech.* **2021**, *3*, 100013. [CrossRef]
23. Wang, H.; Zhu, Y.; Yang, Y.; Zhao, C.; Wu, Y.; Li, T.; Li, J.; Qi, J. Raman spectroscopy study on intergranular corrosion sensitivity of 304 austenitic stainless steel. *Corros. Commun.* **2025**, *20*, 88–92. [CrossRef]
24. Kolli, S.; Javaheri, V.; Ohligschläger, T.; Komi, J.; Porter, D. The importance of steel chemistry and thermal history on the sensitization behavior in austenitic stainless steels: Experimental and modeling assessment. *Mater. Today Commun.* **2020**, *24*, 101088. [CrossRef]
25. Tiamiyu, A.; Eduok, U.; Szpunar, J.; Odeshi, A. Corrosion behavior of metastable AISI 321 austenitic stainless steel: Effect of grain size and prior plastic deformation on degradation in saline media. *Sci. Rep.* **2019**, *9*, 12116. [CrossRef]
26. Petrov, S.N.; Prokoshev, O.Y.; Margolin, B.Z.; Shumko, A.M. Carbide forming special features and fracture mechanisms under the austenitic chromium-nickel 304 steel post-life ageing. *Mater. Phys. Mech.* **2018**, *38*, 111–118.

27. *ASTM A262*; Standard Practices for Detecting Susceptibility to Intergranular Attack in Austenitic Stainless Steels. Annual Book of ASTM Standards; American Society for Testing and Materials: West Conshohocken, PA, USA, 2021.
28. *BS EN ISO 12732*; Corrosion of Metals and Alloys–Electrochemical Potentiokinetic Reactivation Measurement Using the Double Loop Method (DL-EPR). ISO: Geneva, Switzerland, 2010.
29. Číhal, V.; Štefec, R. On the development of the electrochemical potentiokinetic method. *Electrochim. Acta.* **2001**, *46*, 3867–3877. [CrossRef]
30. Číhal, V. *Intergranular Corrosion of Steels and Alloys*; Materials Science Monographs 18; Elsevier: Amsterdam, The Netherlands, 1984.
31. Amadou, T.; Braham, C.; Sidhom, H. Double Loop Electrochemical Potentiokinetic Reactivation Test optimization for assessing duplex stainless steel intergranular corrosion susceptibility. *Metall. Mater. Trans. A* **2004**, *35*, 3499–3513. [CrossRef]
32. Liu, Q.; Qian, J.; Barker, R.; Wang, C.; Neville, A.; Pessu, F. Application of Double Loop Electrochemical Potentio kinetic Reactivation for characterizing the intergranular corrosion susceptibility of stainless steels and Ni based alloys in solar nitrate salts used in CSP systems. *Eng. Fail. Anal.* **2021**, *129*, 105717. [CrossRef]
33. Kuleshova, E.A.; Fedotova, S.V.; Gurovich, B.A.; Frolov, A.S.; Maltsev, D.A.; Stepanov, N.V.; Margolin, B.Z.; Minkin, A.J.; Sorokin, A.A. Microstructure degradation of austenitic stainless steels after 45 years of operation as VVER 440 reactor internals. *J. Nucl. Mater.* **2020**, *533*, 152124. [CrossRef]
34. Suresh, G.; Parida, K.P.; Bandi, S.; Ningshen, S. Effect of carbon content on the low temperature sensitization of 304L stainless steel and its corrosion resistance in simulated groundwater. *Mater. Chem. Phys.* **2019**, *226*, 184–194. [CrossRef]
35. Janda, T.; Jenicek, S.; Kucerova, L.; Letak, R.; Jandova, D.; Jirkova, H. Influence of higher stabilization temperatures on the microstructure and mechanical properties of austenitic stainless steel 08Ch18N10T. *Metals* **2023**, *13*, 975. [CrossRef]
36. Liu, G.; Liu, Y.; Cheng, Y.; Li, J.; Jiang, Y. Intergranular corrosion susceptibility of metastable austenitic Cr–Mn–Ni–N–Cu high strength stainless steel under various heat treatments. *Materials* **2019**, *12*, 1385. [CrossRef]
37. Fang, K.; Luo, K.; Wang, L. Effect of microstructure on mechanical properties of 316LN austenitic stainless steel. *Coatings* **2022**, *12*, 1461. [CrossRef]
38. Dong, Y.; Zhang, Z.; Yang, Z.; Zheng, R.; Chen, X. Effect of annealing temperature on the microstructure and mechanical properties of high-pressure torsion produced 316LN stainless steel. *Materials* **2022**, *15*, 181. [CrossRef]
39. Fang, X.-Y.; Wang, W.-G.; Guo, H.; Zhang, X.; Zhou, B.-X. Corrosion behaviors of random and special grain boundaries in sensitized 304 stainless steels. *J. Iron Steel Res.* **2007**, *14*, 339–343. [CrossRef]
40. Kaneko, K.; Fukanaga, T.; Yamada, K.; Nakada, N.; Kikuchi, M.; Saghi, Z.; Bernard, S.J.; Midgley, A.P. Formation of $M_{23}C_6$ type precipitates and chromium depleted zones in austenitic stainless steel. *Scr. Mater.* **2011**, *65*, 509–512. [CrossRef]
41. Ren, Q.-Q.; Yamamoto, Y.; Brady, P.M.; Poplawski, D.J. Sigma phase evolution and nucleation mechanisms revealed by atom probe tomography in a 347H stainless steel. *Materialia* **2022**, *24*, 101485. [CrossRef]
42. Amirkhiz, B.S.; Xu, S.; Scott, C. Microstructural assessment of 310S stainless steel during creep at 800 °C. *Materialia* **2019**, *6*, 100330. [CrossRef]

Disclaimer/Publisher's Note: The statements, opinions and data contained in all publications are solely those of the individual author(s) and contributor(s) and not of MDPI and/or the editor(s). MDPI and/or the editor(s) disclaim responsibility for any injury to people or property resulting from any ideas, methods, instructions or products referred to in the content.